5 GHz CONTINUUM RADIATION FROM SOUTHERN HEMISPHERE GALACTIC HII REGIONS

By F. F. Gardner* and M. Morimoto†

[*Manuscript received March* 12, 1968]

Summary

The continuum radiation from about 36 southern thermal radio sources has been surveyed at 6 cm wavelength with a beamwidth of 4′·2 arc, and maps are shown for 28 of these. The positional accuracy is better than 1′ arc.

All the sources are resolved to some extent. Peak temperatures, half-intensity widths, and peak emission measures are given for each.

I. Introduction

The 6 cm continuum survey described in the present paper was undertaken mainly to supplement observations currently in progress at the Australian National Radio Astronomy Observatory at Parkes of recombination lines and OH- and H-line emission and absorption. The wavelength is the same as that used in a similar survey by Mezger and Henderson (1967) in the northern hemisphere, but the beamwidth is 50% narrower (4′·2 arc compared with 6′·4 arc). While the emphasis was on the strongest thermal sources‡ in the southern sky, there are 10 sources in common with Mezger and Henderson. As in the latter survey, the interest has been in the brightest concentrations for which peak antenna temperatures are measured and (to a lesser degree of accuracy) the brightness temperatures, fluxes, and emission measures derived. Distance estimates for the HII regions are not considered in the present paper.

II. Telescope and Equipment

The observations were made in May 1967 with the Parkes 210 ft telescope. The reflecting surface consists of an inner 55 ft of solid surface surrounded by 1380 mesh panels. With the aid of a special survey instrument these panels were set so that the shape was optimum near zenith angle 30° (Minnett, Yabsley, and Puttock 1967). This minimized the variation in performance over the normal range of zenith angle, and in fact point source measurements with fixed focus showed that the gain, including extinction, exceeded 95% of its peak value in the range 20° to 55°, where practically all observations in the present paper were made. In practice, the gain variation was less than this, as the focus was adjusted to the value appropriate to the mean zenith angle for each source.

The feed system consisted of a dual-mode circular horn similar to one used previously at 18 cm wavelength (Gardner, McGee, and Robinson 1967). This pro-

* Division of Radiophysics, CSIRO, P.O. Box 76, Epping, N.S.W. 2121.

† This work was performed during the tenure of a CSIRO fellowship at the Division of Radiophysics, CSIRO, P.O. Box 76, Epping, N.S.W. 2121. Present address: Tokyo Astronomical Observatory, Tokyo, Japan.

‡ Listed by Westerhout (1958) and Mathewson, Healey, and Rome (1962).

duced a circular feed beam with low spillover and, within the accuracy of measurement, a circular secondary beam. The illumination taper was somewhat greater than in the preliminary 6 cm observations (Broten *et al.* 1965) and as a result the half-intensity beamwidth of $4'\cdot 2$ arc was slightly greater than before.

The radiometer was switched at 40 Hz between the feed and a liquid-nitrogen-cooled termination. Approximate noise balance was achieved by adding noise to the signal side. The receiver consisted of a tunnel diode input stage followed by a double-sideband mixer with an intermediate-frequency band from 5 to 100 MHz. The input bandwidth was twice this, covering $4\cdot 9$–$5\cdot 1$ GHz. The overall noise temperature was around 800°K.

The 10°K calibration used in the observations was obtained from a noise lamp through an adjustable attenuator and a directional coupler. It was set by reference to a thermal calibration in which the load temperature was changed from 0°C to 50°C.

The brightness temperature scale was determined from measurements of the beam shape for small diameter sources and from a measurement of the ratio of the peak response (mean of two orthogonal polarizations) to the calibration for the quasi-stellar source 3C 273 (assuming that the flux of 3C 273 at the time of observation, mid May 1967, was 41 f.u.). On the same scale Hydra A and M 87 had peak flux values of 13 and 69 f.u. respectively.

For a Gaussian beamshape with half-intensity width B, an extended region of brightness temperature T_b will give the same radiometer output as a point source of flux S if

$$T_b/S = 3\cdot 77\times 10^3(\lambda/B)^2 = 0\cdot 77$$

in our case, with λ in metres and B in minutes of arc. The corresponding antenna temperature T_a for a 210 ft paraboloid with aperture efficiency η_a is

$$T_a/S = 1\cdot 165\eta_a \qquad \text{or} \qquad T_b/T_a = 0\cdot 66/\eta_a .$$

With T_a derived from the thermal calibration, as outlined earlier, $T_b/T_a \simeq 2\cdot 0$ and correspondingly $\eta_a = 0\cdot 33$. This includes atmospheric extinction under good conditions at a zenith angle of $\sim 35°$.

III. Observational Method

The main observations were generally drift scans at declination intervals of $2'\cdot 0$ arc. At least two scans were made and averaged for each declination and if there was any obvious difference between them a third scan was made. Forward and reverse scans in declination at $0\cdot 25$ deg/min were made through the source peak position and also as tie-in scans at right ascensions away from steep gradients in intensity. At declinations below $-50°$ the right ascension scans were made with the telescope driving at about $+0\cdot 25 \sec\delta$ deg/min. The time constant of 1 sec was allowed for in the reduction, which was done from the analogue charts. The sensitivity was generally governed by receiver drifts and fluctuations in sky background rather than by receiver noise. Extinction corrections for "good-seeing" conditions are included in the calibration.

In all cases the accuracy of pointing of the telescope was better than 1′ arc. Average refraction is compensated for in the error detection system (Bolton, Gardner, and Mackey 1964).

IV. Results

The results of the survey are presented in Figures 1(*a*)–1(*w*) and Table 1. Column (1) of the table gives the source name. If available, the optical number is given precedence—Messier, NGC, or RCW (Rodgers, Campbell, and Whiteoak 1960); otherwise the Westerhout (W) number or a coordinate number as used in the Parkes catalogue (Bolton, Gardner, and Mackey 1964) is used. Columns (2) and (3) give the source peak position in celestial and galactic coordinates. Column (4) gives the observed widths θ'_α and θ'_δ in minutes of arc and column (5) gives the derived widths θ_α and θ_δ of the components under the assumption of Gaussian source and beam. Column (6) gives antenna temperature T_a, column (7) the flux S, column (8) the central brightness temperature T_b derived for a Gaussian model, and column (9) the corresponding central emission measure.

The conversion from θ'_α to θ_α is through the formula

$$(\theta'_\alpha)^2 = \theta_\alpha^2+(4\cdot2)^2\,.$$

The flux S is given by

$$S = S_{\max}\,\theta'_\alpha\,\theta'_\delta/(4\cdot2)^2\,,$$

and the central brightness temperature T_b for a Gaussian model by

$$T_b = T_{b,\max}\,\theta'_\alpha\,\theta'_\delta/\,\theta_\alpha\,\theta_\delta \simeq 2T_a\,\theta'_\alpha\,\theta'_\delta/\,\theta_\alpha\,\theta_\delta\,.$$

Here $T_{b,\max}$ is the peak chart deflection measured in terms of the full-beam brightness temperature scale.

The formula of Scheuer (1960) or equation (5) of Mezger and Henderson (1967) relates T_b and emission measure E.M. in pc cm^{-6}. For 5·0 GHz

$$T_b = (\mathrm{E.M.})\times1\cdot10\times10^{-4}\,.$$

For a number of multiple-component sources the individual components cannot be clearly separated from the surrounding background, and the fluxes derived will depend on the beamwidth and on assumptions about the underlying background.

V. Discussion

When a comparison is made with the results of Mezger and Henderson (1967) for the sources in common, it is found that most of our values of flux are lower and emission measures higher for the central components. This is probably just the result of the 50% greater resolution, and it is likely that the trend would continue with further increase in resolution, as was found by Mezger, Schraml, and Terzian (1967) to be the case for W 49.

Six of the sources shown in Figures 1(*a*)–1(*w*) are associated with strong OH emission, namely PKS 1308−62, PKS 1608−51, PKS 1617−50, NGC 6334, W 49,

TABLE 1

PARTICULARS OF CONTINUUM SOURCES AT 6 CM

(1) Source	(2) Position (1950·0) R.A. h m s	Dec. ° ′	(3) Galactic Coordinates l^{II} °	b^{II} °	(4) Observed Widths R.A. θ'_α ′	Dec. θ'_δ ′	(5) Source Widths R.A. θ_α ′	Dec. θ_δ ′	(6) Antenna Temperature T_a (°K)	(7) S (f.u.)	(8) Central Brightness Temperature T_b (°K)	(9) Emission Measure (10^5 pc cm^{-6})	(10) Remarks
Orion A	05 32 50	−05 25·4	209·0	−19·4	5·33	5·43	3·28	3·45	80·8	344	414	37·6	
NGC 2024	05 39 09	−01 56·1	206·5	−16·4	5·36	5·00	3·3	2·7	13·8	57·5	82	7·4	
RCW 38	08 57 18	−47 19·2	267·9	− 1·1	4·75	4·82	2·2	2·35	54·5	183	482	43·7	
RCW 36	08 57 35	−43 33·9	265·1	+ 1·4	5·05	5·00	2·8	2·7	6·9	26·6	46	4·2	
RCW 46	10 04 52	−56 57·7	282·0	− 1·2	4·84	4·80	2·4	2·4	8·2	28·0	66	6·0	
RCW 49	10 22 18	−57 32·1	284·3	− 0·3	6·76	7·9	5·3	6·7	24·2	190	73	6·6	
Carina nebula	10 41 32	−59 19·7	287·3	− 0·6	7·0	9·0	5·6	8·0	13·5	125	38	3·4	
	10 42 48	−59 23·7	287·8	− 0·6	9·7	5·8	8·7	4·0	12·4	103	40	3·6	
RCW 57	11 09 41	−61 02·3	291·3	− 0·7	4·56	4·72	1·8	2·2	31·6	100	343	31·1	
	11 12 46	−60 59·2	291·6	− 0·5	6·09	7·75	4·4	6·5	24·1	167	79	7·1	
PKS 1207−62	12 07 19	−62 33·4	298·2	− 0·3	4·72	4·5	2·2	1·6	8·5	26·5	102	9·2	
PKS 1308−62	13 08 10	−62 29·5	305·2	+ 0·0	7	7	5·6	5·6	3·5	25·2	11	1·0	RCW 74
	13 08 15	−62 18·9	305·2	+ 0·2	6·5	7	5·0	5·6	5·5	36·6	18	1·6	
	13 09 16	−62 18·8	305·3	+ 0·2	6	5	4·3	2·7	9·2	40·6	47	4·3	
	13 11 04	−62 29·1	305·5	+ 0·0	~6	5·5	4·3	3·5	1·6	7·8	7	0·6	
PKS 1441−59	14 41 29	−59 37·0	316·8	− 0·05	5·1	5·0	2·9	2·7	9·4	34·1	61	5·5	
PKS 1442−59	14 42 00	−59 12·5	317·0	+ 0·3	~10	~8·5			1·4	~17·5	~3	~0·3	
PKS 1540−54	15 40 47	−53 57·2	326·7	+ 0·6	5·0	6·3	2·7	4·7	8·8	40·7	44	4·0	Contains smaller core
PKS 1549−54	15 49 12	−54 26·3	327·3	− 0·5	4·79	4·40	2·3	1·3	15	48·1	220	19·9	Core only; broad ext. to S. and W.
PKS 1608−51	16 08 19	−51 19·2	331·5	− 0·1	5·03	4·74	2·8	2·2	9·1	31·8	70	6·3	
						4·98*		2·7*		33·6			

Norma sources	16 15 55	−50 56·1	332·6	− 0·6	5·0	5·0	2·7	2·7	4·3	15·8	29	2·6	
	16 16 19	−50 48·7	332·8	− 0·5	6	7	4·3	5·6	3·0	18·5	10	0·9	
	16 16 51	−50 32·9	333·0	− 0·5	5·5	4·5	3·6	1·6	6·8	24·7	58	5·2	
	16 17 13	−50 30·4	333·1	− 0·5	5·5	5·5	3·6	3·6	8·3	36·8	39	3·5	
	16 17 43	−50 20·5	333·3	− 0·4	4·8	5·0	2·4	2·7	10·0	35·2	74	6·7	
	16 18 23	−49 59·5	333·6	− 0·2	4·75	4·5	2·2	1·6	25·7	80·9	313	28·3	
PKS 1630−47	16 30 48	−47 30·0	336·8	+ 0·1	10·9	8·4	10·0	7·4	4·6	61·9	11	1·0	Another component at R.A. $16^h 33^m 20^s$
PKS 1636−46	16 36 27	−46 16·2	338·4	+ 0·2	6·0	7·5	4·3	6·2	3·9	25·8	13	1·2	
	16 37 07	−46 17·5	338·4	+ 0·1	7·2	9·5	5·8	8·5	5·2	52·3	14	1·3	
PKS 1716−38	17 16 38	−38 55·1	348·7	− 1·0	4·95	4·9	2·6	2·5	11	39·3	82	7·4	
NGC 6334	17 16 26	−36 03·0	351·0	+ 0·7	7·6	7·8	6·3	6·6	4·7	40·9	13	1·2	
	17 17 18	−35 47·1	351·3	+ 0·7	—	—			14·2		>40	>3·6	Ridge of small diam. sources at $b^{II} = 0°·7$
	17 17 31	−36 01·1	351·2	+ 0·5	5·8	4·5	4·0	1·6	3·9	14·9	31	2·8	
NGC 6357	17 21 24	−34 08·1	353·2	+ 0·9	7·0	5·2	5·6	3·1	22·5	120	94	8·5	
	17 22 15	−34 20·1	353·1	+ 0·6	9·2	8·0	8·2	6·8	16	67·5	42	3·8	
	17 23 21	−34 31·1	353·1	+ 0·4					3·6		10	0·9	
M 8	18 00 38	−24 23·0	6·0	− 1·2	5·5	5·5	3·6	3·6	10	44·5	47	4·3	Ext. component removed
W 31	18 06 04	−20 04·2	10·3	− 0·1	5·0	6·0	2·7	4·3	5·1	22·4	27	2·4	
	18 06 28	−20 19·8	10·2	− 0·4	5·47	4·5	3·5	1·6	14·0	50·9	123	11·1	
	18 07 34	−19 56·8	10·6	− 0·4	5·8	5·0	4·0	2·7	2·3	9·8	12	1·1	
M 16	18 15 38	−13 44·2	17·0	+ 0·9	10	10	9·1	9·1	2·9	42·6	7	0·6	
	18 16 09	−13 51·6	16·9	+ 0·7	9	10	8·0	9·1	3·4	45·0	9	0·8	
M 17	18 17 40	−16 13·0	15·0	− 0·7	5·9	7·5	4·15	6·2	66	430	227	20·6	Ext. component removed
W 43	18 45 02	−01 58·9	30·8	− 0·0	6·1	6·4	4·4	4·8	16	91·7	65	5·9	Ext. component removed
W 49	19 07 52	+09 00·7	43·2	+ 0·0	5·26	4·50	3·2	1·6	15·7	54·7	145	13·1	
	19 08 44	+09 00·5	43·3	− 0·2	5·73	5·13	3·9	2·7	4·9	21·2	26		
W 51	19 20 04	+13 58·4	48·9	− 0·3	7·5	11	6·2	10·1	4·8	58·3	13	1·2	
	19 20 37	+14 02·0	49·1	− 0·4					3·9		10	0·9	
	19 20 44	+14 09·5	49·2	− 0·4	5·7	5·0	3·9	2·7	6	25·2	32	2·9	
	19 20 55	+14 20·8	49·4	− 0·3	5·4	5·0	3·4	2·7	7	27·8	41	3·7	
	19 21 25	+14 24·2	49·5	− 0·4	5·3	5·0	3·2	2·7	28	109	168	15·2	

* Background not subtracted.

and W 51. For five of these, the OH positions (Gardner, McGee, and Robinson 1967; McGee, Gardner, and Robinson 1967; Weaver *et al.* 1968) are displaced to the edge of the thermal source—in most cases to a distance where the emission (when corrected for beam broadening) would be below one-quarter of the central intensity. That is, the OH emission is from near the edge of the HII region, as expected for the simple model discussed by Gardner, McGee, and Robinson in connection with NGC 6334. For W 49, our resolution is inadequate for any meaningful comment, but Mezger, Schraml, and Terzian (1967) find that only one of the two OH components is near the periphery of the source. For the source IC 1795, which is not visible from Parkes, Rogers *et al.* (1967) have found that the OH emission is again from the outer edge of the intense HII region, but Mezger *et al.* (1967) have found a weak source in approximate coincidence with the OH-emission position. Our resolution is insufficient to rule out the possibility of similar weak continuum sources coincident with the OH positions for the other sources listed above.

The map of the Carina nebula shows two components separated by some 10′ arc along a line of constant galactic latitude. The similarity in peak intensity and angular size of the two components suggests that they are parts of the same object. However, 126 α and 127 α hydrogen recombination line profiles observed by McGee and Gardner (1968) are very different for the two components. The western component has a normal line-to-continuum ratio and width, and its central velocity of -20 km sec^{-1} is that expected from the galactic rotation model. However, the eastern component, nearer to the peculiar star η Carinae, has a lower line-to-continuum ratio and the profile is very broad and appears to be composed of two components with mean velocities of 0 and -40 km sec^{-1}. Future high resolution recombination line mapping of the nebula should be very useful for revealing the details of these large internal motions.

VI. Conclusions

Twenty-eight HII regions have been mapped with a $4'\cdot 2$ arc beam and individual components with angular diameter down to $1'\cdot 5$ have been found. It is quite likely that finer detail would emerge with more resolution. To this extent the peak emission measures quoted should be considered only as lower limits.

A comparison between positions of OH and continuum features indicates that in five out of six cases the OH emission originates from the periphery of the HII region. For these five cases higher resolution mapping would be required to reveal the presence of weak continuum features coincident with the OH-emission position.

VII. Acknowledgments

The authors are indebted to Miss J. Milton and Miss M. Adams for their assistance with the data reduction, and to Mr. F. Tonking who was responsible for the design and construction of the radiometer.

Figs. 1(a)–1(w).—Contour maps of galactic radio sources at $\lambda = 6$ cm. The scale is shown for each map and asterisks indicate OH-emission positions.

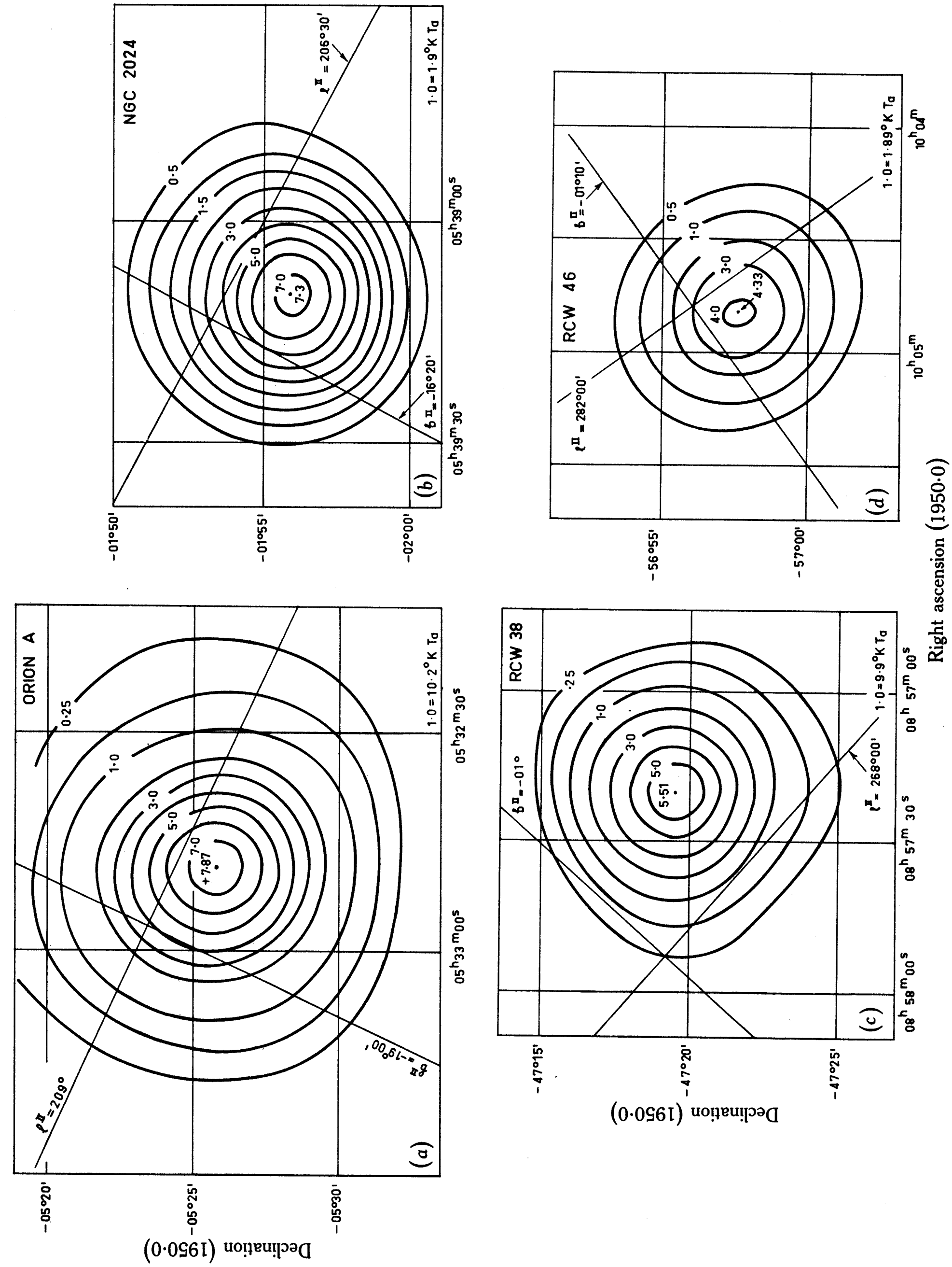
(a)
ORION A
1·0 = 10·2°K Ta
+7·87
7·0
5·0
3·0
1·0
0·25
ℓ^{II} = 209°
b^{II} = −19°00′
05h33m00s
05h32m30s
−05°20′
−05°25′
−05°30′
Declination (1950·0)
(b)
NGC 2024
1·0 = 1·9°K Ta
7·0
7·3
5·0
3·0
1·5
0·5
ℓ^{II} = 206°30′
b^{II} = −16°20′
05h39m30s
05h39m00s
−01°50′
−01°55′
−02°00′
(c)
RCW 38
1·0 = 9·9°K Ta
5·51
5·0
3·0
1·0
·25
ℓ^{II} = 268°00′
b^{II} = −01°
08h58m00s
08h57m30s
08h57m00s
−47°15′
−47°20′
−47°25′
Declination (1950·0)
(d)
RCW 46
1·0 = 1·89°K Ta
4·33
4·0
3·0
1·0
0·5
ℓ^{II} = 282°00′
b^{II} = −01°10′
10h05m
10h04m
−56°55′
−57°00′
Right ascension (1950·0)

Figs. 1(a)–1(d)

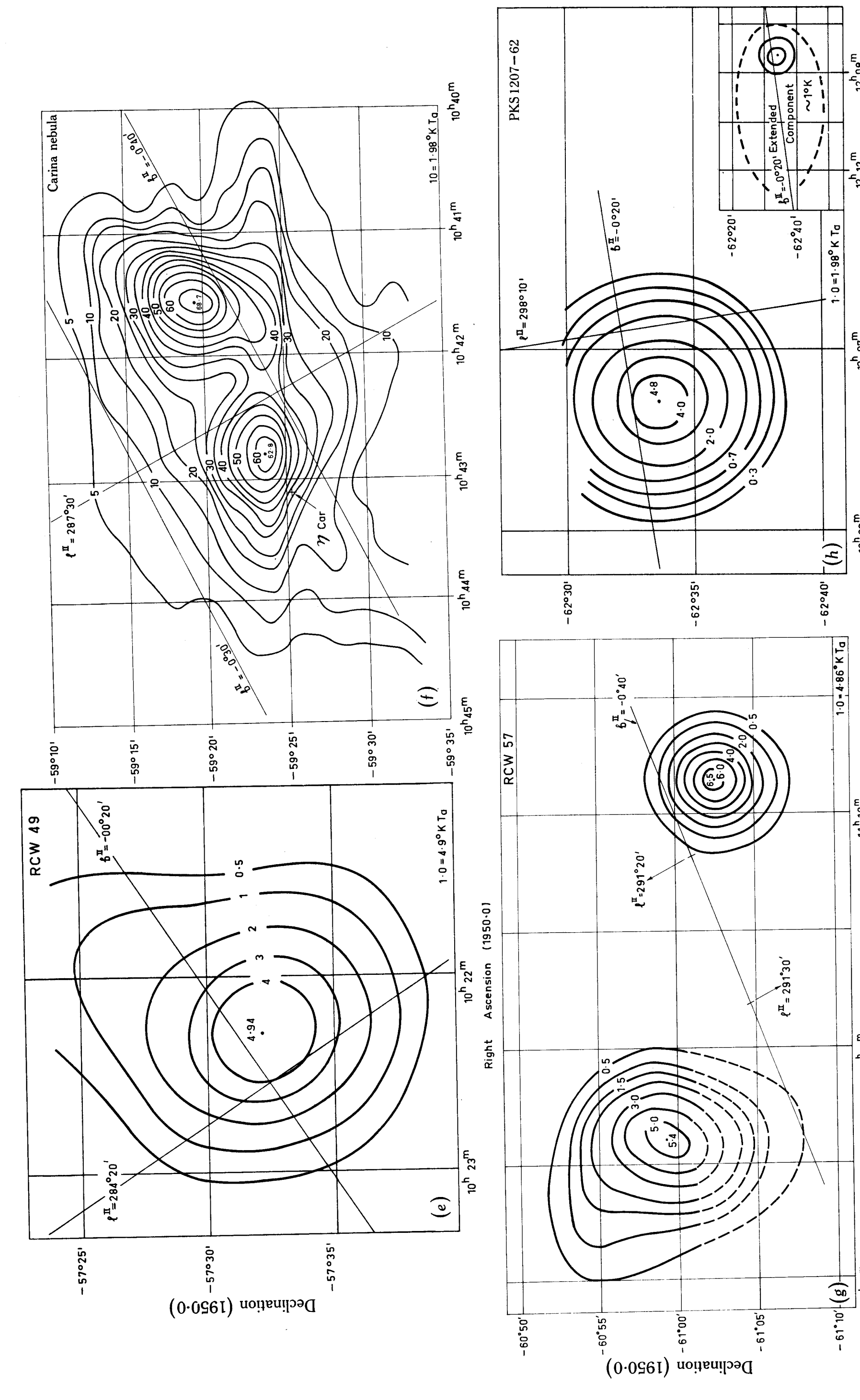

Right ascension (1950·0)

Figs. 1(*e*)–1(*h*)

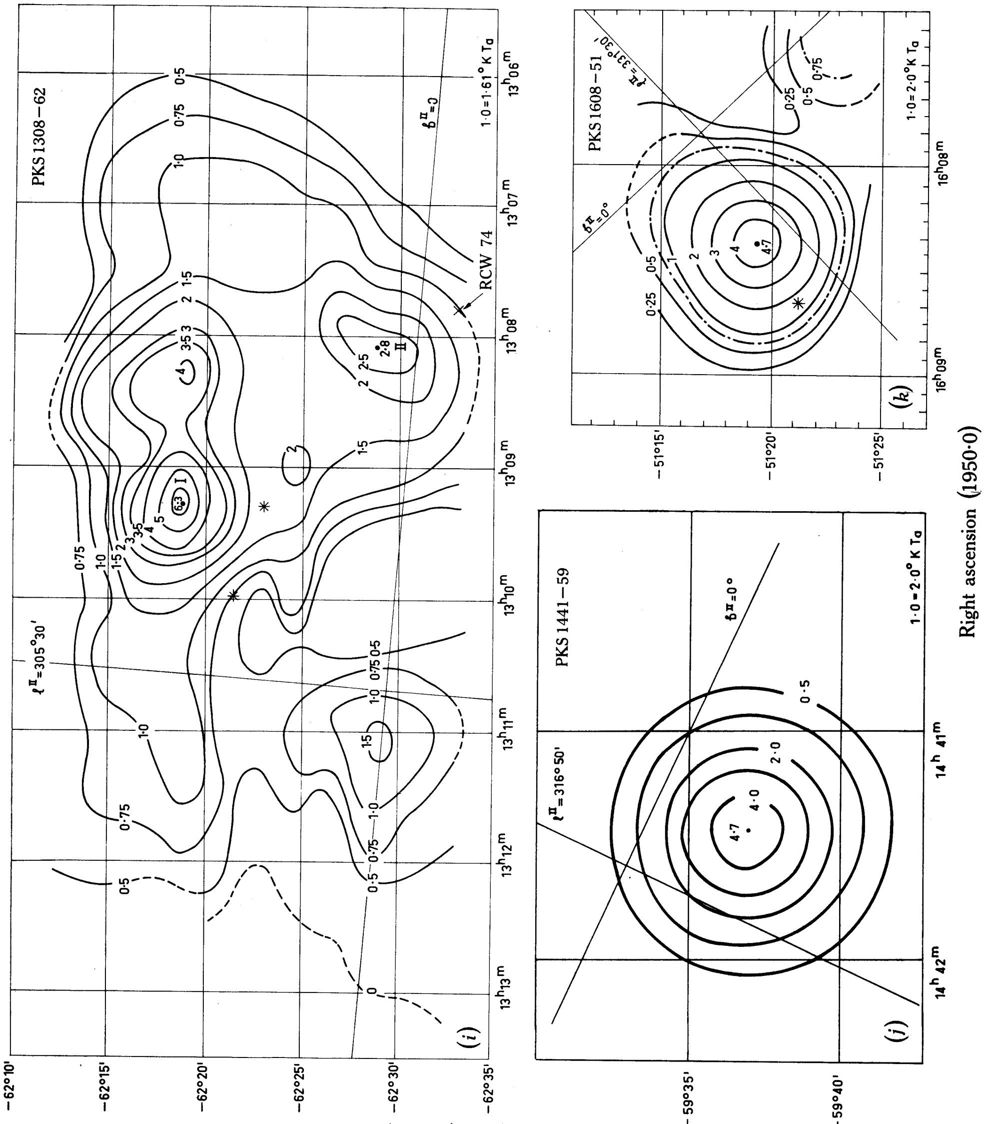

Figs. 1(*i*)–1(*k*).—The asterisks in (*i*) and (*k*) indicate OH emission.

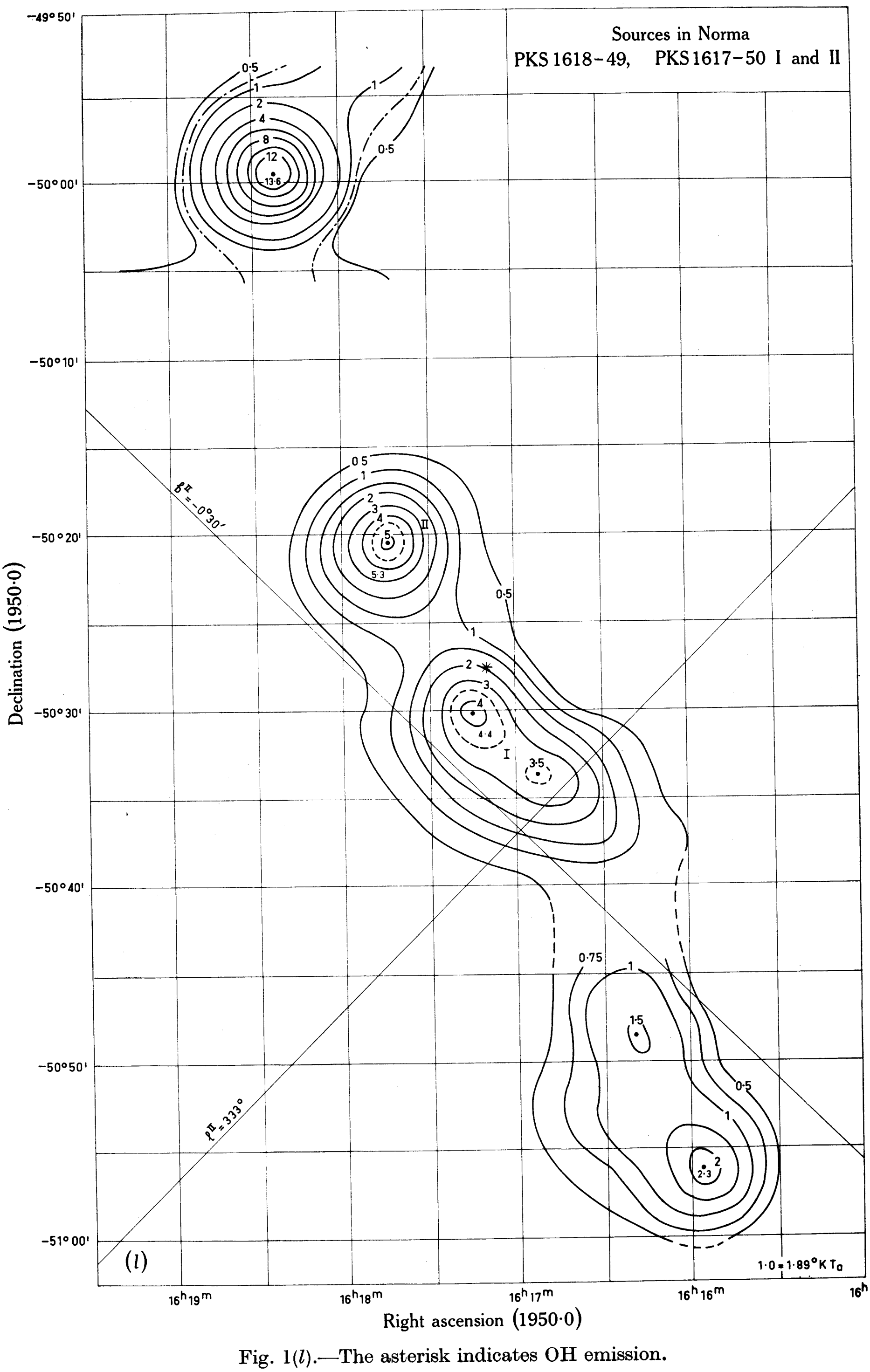

Fig. 1(*l*).—The asterisk indicates OH emission.

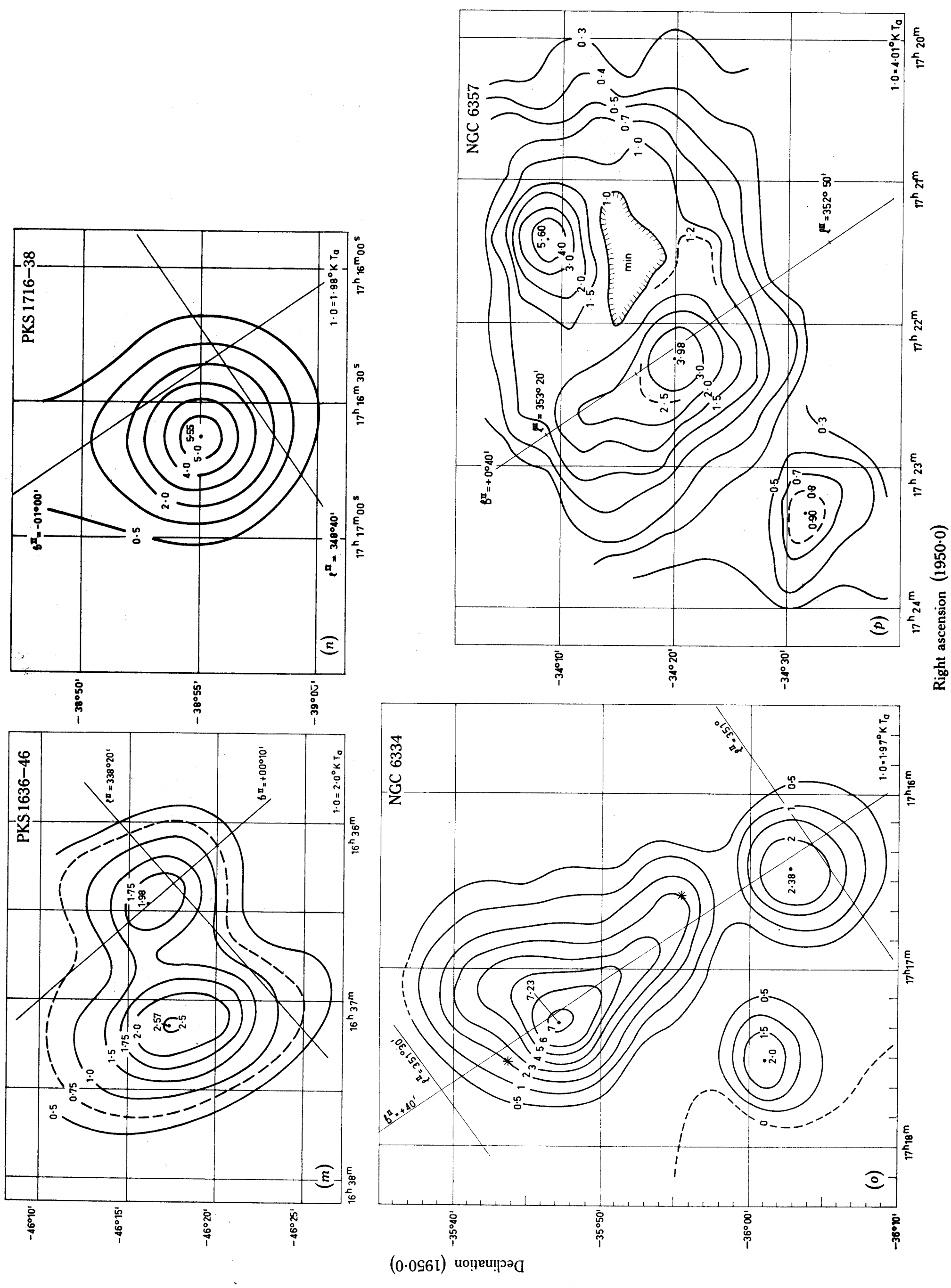

Figs. 1(*m*)–1(*p*).—The asterisks in (*o*) indicate OH emission.

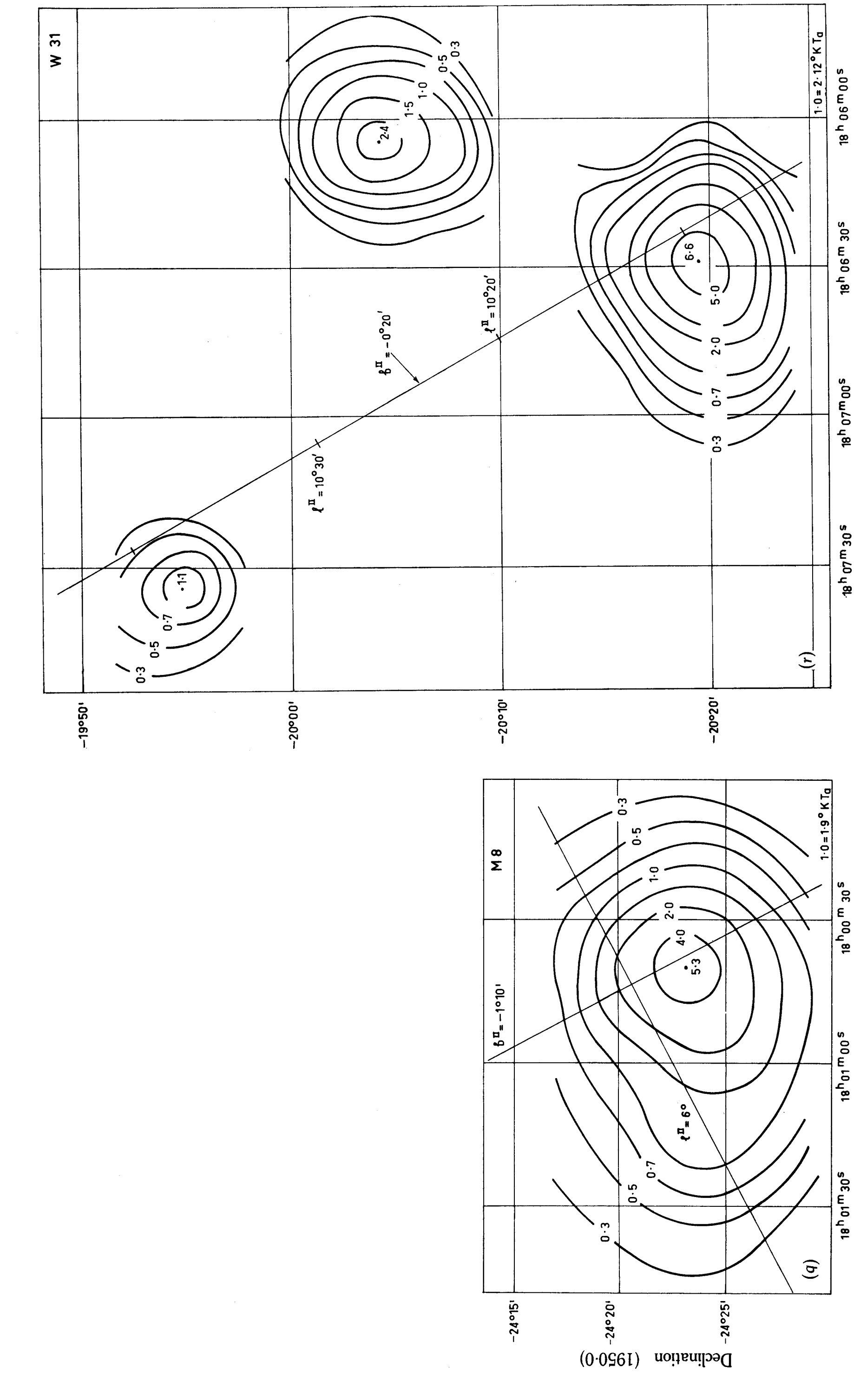

Figs. 1(q) and 1(r)

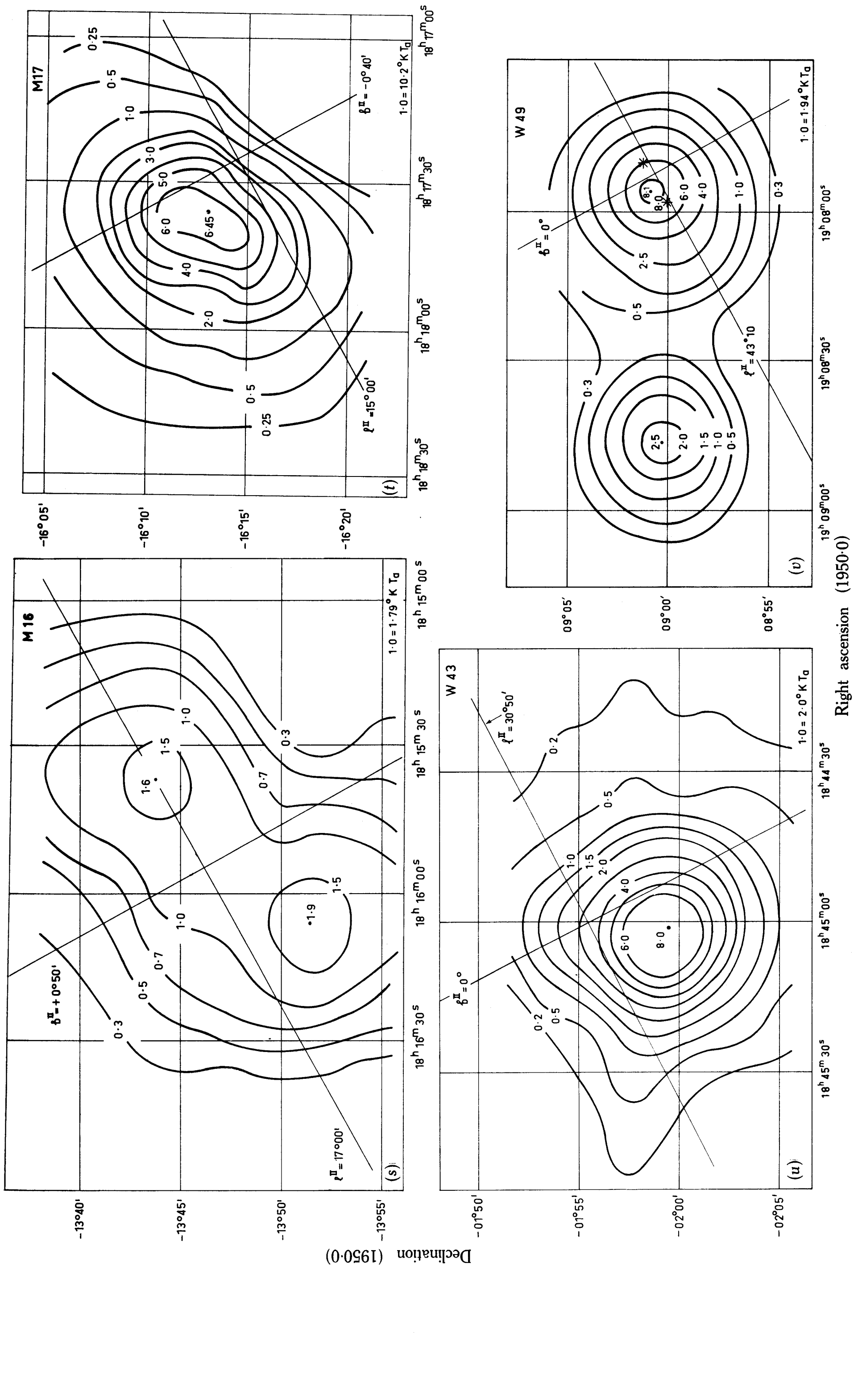

Figs. 1(*s*)–1(*v*).—The asterisks in (*v*) indicate OH emission.

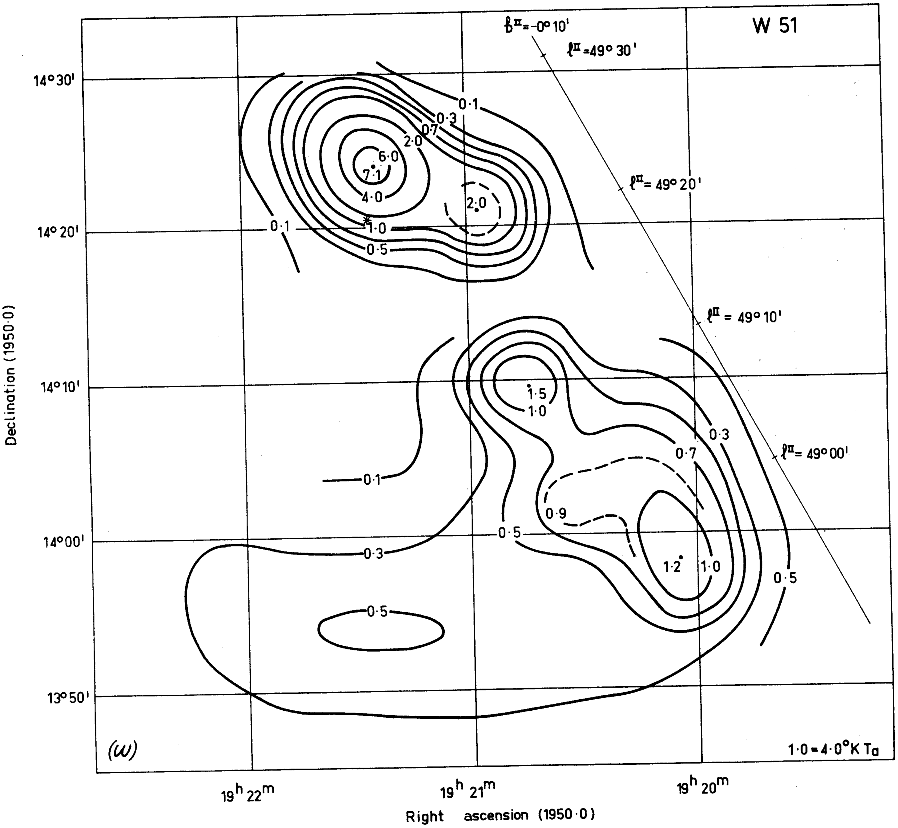

Fig. 1(w).—The asterisk indicates OH emission.

VIII. References

Bolton, J. G., Gardner, F. F., and Mackey, M. B. (1964).—*Aust. J. Phys.* **17**, 340–72.

Broten, N. W., Cooper, B. F. C., Gardner, F. F., Minnett, H. C., Price, R. M., Tonking, F. G., and Yabsley, D. E. (1965).—*Aust. J. Phys.* **18**, 85–90.

Gardner, F. F., McGee, R. X., and Robinson, B. J. (1967).—*Aust. J. Phys.* **20**, 309–24.

McGee, R. X., and Gardner, F. F. (1968).—*Aust. J. Phys.* **21**, 149–66.

McGee, R. X., Gardner, F. F., and Robinson, B. J. (1967).—*Aust. J. Phys.* **20**, 407–20.

Mathewson, D. S., Healey, J. R., and Rome, J. M. (1962).—*Aust. J. Phys.* **15**, 354–68.

Mezger, P. G., *et al.* (1967).—*Astrophys. J.* **150**, L157–66.

Mezger, P. G., and Henderson, A. P. (1967).—*Astrophys. J.* **147**, 471–89.

Mezger, P. G., Schraml, J., and Terzian, Y. (1967).—*Astrophys. J.* **150**, 807–23.

Minnett, H. C., Yabsley, D. E., and Puttock, M. J. (1967).—Structural performance of the Parkes 210-ft paraboloid. Proc. Int. Symp. on Structures Technology for Large Radio and Radar Telescope Systems, Mass. Inst. of Technology, October 18–20, 1967 (in press).

Rodgers, A. W., Campbell, C. T., and Whiteoak, J. B. (1960).—*Mon. Not. R. astr. Soc.* **120**, 1–8.

Rogers, A. E. E., *et al.* (1967).—*Astrophys. J.* **147**, 369–76.

Scheuer, P. A. G. (1960).—*Mon. Not. R. astr. Soc.* **120**, 231–41.

Weaver, H., Dieter, Nannielou H., and Williams, D. R. (1968).—*Astrophys. J. Suppl. Ser.* **16**, No. 146.

Westerhout, G. (1958).—*Bull. astr. Insts Neth.* **14**, 215–60.